Mineralogical Magazine (2024), 1–14
doi:10.1180/mgm.2024.22

CAMBRIDGE UNIVERSITY PRESS

Article

Electron density changes accompanying high-pressure phase transition in AlOOH

Roman Gajda[1], Jan Parafiniuk[2], Pierre Fertey[3], Przemysław Dera[4,1] and Krzysztof Woźniak[1]

[1]Biological and Chemical Research Centre, Department of Chemistry, University of Warsaw, Żwirki i Wigury 101, Warszawa, 02-089, Poland; [2]Institute of Geochemistry, Mineralogy and Petrology, Department of Geology, University of Warsaw, Żwirki i Wigury 93, Warszawa, 02-089, Poland; [3]Synchrotron SOLEIL, L'Orme des Merisiers - Saint Aubin, B.P. 48, Gif-sur-Yvette Cedex 91 192, France; and [4]Hawai'i Institute of Geophysics and Planetology, University of Hawai'i at Manoa, 1680 East-West Road, Honolulu, Hawai'i, USA

Abstract

An attempt to compare and describe the differences in the electron density distribution between two phase structures of AlOOH has been made. High-resolution, high-pressure experiments with α-AlOOH diaspore were conducted using single-crystal synchrotron X-ray diffraction data. A multipole model of experimental electron density in the α-AlOOH single crystal was refined. Simultaneously, similar multipole refinement was conducted for another phase of diaspore (δ-AlOOH), this time based on a previously published data set. Both results were compared and supported by density functional theory (DFT) calculations. Although the results are affected by the limited quality of the data, it is clear that the phase transition caused significant changes in the shape and arrangement of the atomic basins.

Atomic basins are a much better tool to present subtle electron density distribution changes than traditional polyhedra. Straightforward comparison of datasets available in older scientific papers and current datasets is challenging because of differences in data quality and collection parameters. However, augmenting experimental data with computational results can help reveal important information in even incomplete datasets.

Keywords: electron density; phase transition; high pressure; oxyhydroxides

(Received 16 January 2024; accepted 20 March 2024; Accepted Manuscript published online: 11 April 2024; Associate Editor: G. Diego Gatta)

Introduction

Compounds that belong to the oxyhydroxide group (M^{3+}OOH, M = Al, Sc, V, Cr, Mn, Fe, Ga, Rh and In) have been investigated widely under non ambient conditions, such as high pressure (HP) and/or variable temperature (Li *et al.*, 2010; Sano-Furukawa *et al.*, 2012; Suzuki, 2013, 2018; Zhang *et al.*, 2017; Shito *et al.*, 2019; Tang *et al.*, 2020; Ito *et al.*, 2022). A common phase transition sequence observed in this group is from the diaspore-type structure (α-AlOOH, *Pnma*) at ambient pressure to a high pressure InOOH-type structure ($Pmn2_1$) (see Figs 1 and 2), and then further to the YOOH-type structure ($P2_1/m$) (Bolotina *et al.*, 2008; Ito *et al.*, 2021). The exact values of the transition pressures between the α-AlOOH-type and InOOH-type and then between the InOOH-type and YOOH-type differ significantly depending on the composition. For example, the transitions between the α-AlOOH-type and the InOOH-type for GaOOH, AlOOH and ScOOH occurs at 8.5 GPa, 18.0 GPa, and 4.4 GPa, respectively but the phase transition from the InOOH-type to the YOOH-type for InOOH and ScOOH occurs at 50.8 GPa and 8.1 GPa, respectively (Ito *et al.*, 2021).

From a mineralogical perspective, (M^{3+}OOH) oxyhydroxide minerals are interesting as potential carriers of water into the Earth's lower mantle (Verma *et al.*, 2018). The deep Earth mantle was originally thought to be devoid of water due to the observed decomposition of hydrous minerals at high temperatures and pressures at depths of ~150 km (5 GPa). Recent discoveries, however, have revealed hydrous minerals stable at much greater pressures, some retaining water even in the lower mantle. Researchers are now actively investigating the high-pressure behaviours of dense hydrous magnesium silicates, including phases A, superhydrous phase B, phase D and phase H, to understand their role in the deep Earth's water cycle (Xu *et al.*, 2021; Li *et al.*, 2022).

Diaspore is also a mineral of practical importance. Cryptocrystalline or earthy diaspore is an important component of bauxite, the most important aluminium ore. It forms as the final product of intense weathering of various types of rocks. Its prismatic or tabular crystals are found in some alkali pegmatites and products of hydrothermal alteration of aluminosilicate minerals. Transparent, well-formed diaspore crystals, that sometimes change colour under different lighting, are cut as gemstones ('zultanite').

The first crystallographic investigations of diaspore were performed almost a century ago (Ewing, 1935; Busing and Levy,

Corresponding authors: Roman Gajda; Email: romanbg@chem.uw.edu.pl; Krzysztof Woźniak; Email: kwozniak@chem.uw.edu.pl

Cite this article: Gajda R., Parafiniuk J., Fertey P., Dera P. and Woźniak K. (2024) Electron density changes accompanying high-pressure phase transition in AlOOH. *Mineralogical Magazine* 1–14. https://doi.org/10.1180/mgm.2024.22

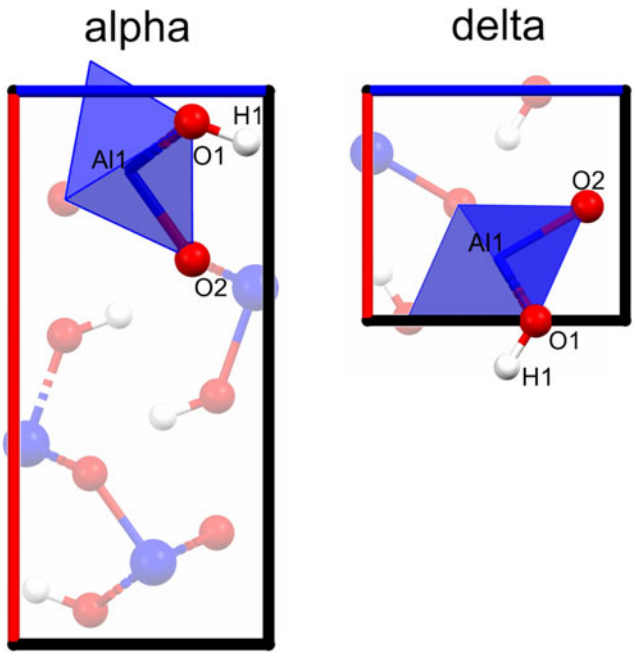

Figure 1. Atoms within the asymmetric part of the unit cell inscribed in the shape of the AlO_6 polyhedra. View along the y-axis.

1958). α-AlOOH diaspore is the thermodynamically stable phase at low pressure. Under equilibrium conditions (high temperature) it transforms to δ-AlOOH above 18 GPa (Suzuki *et al.*, 2000; Komatsu *et al.*, 2006; Simonova *et al.*, 2020), but when compressed at ambient temperature, it metastably retains the original structure to pressures as high as 50 GPa (Friedrich *et al.*, 2007b). Diaspore crystallises in space group 62. In the ICSD [Inorganic Crystal Structure Database, https://icsd.products.fiz-karlsruhe.de/] all deposited diaspore structures are described in *Pbnm*, however the alternative, equivalent *Pnma* setting better complies with the current IUCr edition of *International Tables for Crystallography* (Hahn, 2002). The stability of this structure within various pressure ranges and potential phase transitions has already been investigated widely by various groups (Xu *et al.*, 1994; Pawley *et al.*, 1996; Grevel *et al.*, 2000; Friedrich *et al.*, 2007a; 2007b; Cedillo *et al.*, 2016; Sugiura *et al.*, 2018; Huang *et al.*, 2021).

δ-AlOOH has been investigated systematically and its equilibrium *p*–*T* phase boundary with diaspore has been established (Sano-Furukawa *et al.*, 2009). The differences in compressibility between δ-AlOOH and the deuterated form δ-AlOOD have also been studied (Suzuki, 2022). It is known that δ-AlOOH undergoes further subtle phase transitions at pressures from 6.1 to 8.2 GPa (Kuribayashi *et al.*, 2014). Dense hydrous magnesium silicates within subducting slabs undergo a phase transition leading to formation of a mixture of H_2O and anhydrous minerals. δ-AlOOH, however, has demonstrable stability within the lower mantle's pressure–temperature conditions, though questions remain about its behaviour in the lowermost mantle, where temperature increases rapidly with depth. Its thermodynamic stability extends to pressures and temperatures up to 134 GPa and 2300 K, with theoretical predictions suggesting a transition to a pyrite-type structure above 170 GPa, confirmed experimentally at ~190 GPa (Ohira *et al.*, 2014). However, the formation of pyrite-type AlOOH remains unverified, highlighting the need for further high-pressure, high-temperature experiments. Recent high-pressure experiments propose that δ-AlOOH, which is structurally similar to phase H, could remain stable in the lower mantle (Thompson *et al.*, 2021). It has also been shown that Al can separate from bridgmanite and $CaSiO_3$ perovskite to form δ-AlOOH in the presence of H_2O. Thus, δ-AlOOH is a promising candidate as a primary carrier of water deep within the Earth.

The first study describing electron density distribution in diaspore (α-AlOOH) was published in 1979 (Hill, 1979), in which, on the basis of 597 reflections, the valence expansion/contraction coefficients, as well as atomic charges were estimated. In this paper, we compare electron density distribution in the α-AlOOH and δ-AlOOH phases. In this study we performed a new high-pressure, high-resolution synchrotron XRD experiment at 2.5 GPa, and analysed these experimental data using multipole refinement of electron density according to the Hansen–Coppens model (Hansen and Coppens, 1978; Coppens *et al.*, 1979). We have also optimised the structure of α-AlOOH by DFT calculations using *CRYSTAL17* software (Dovesi *et al.*, 2005, 2018). Calculated on the basis of this optimisation, dynamical structure factors ($\tilde{F}_{hkl}$) (Erba *et al.*, 2013) have allowed us to obtain theoretical electron density distributions, which can be used as a benchmark for experimental results. Furthermore, to test the reusability of older X-ray data sets and their usefulness in more advanced modern quantum crystallographic approaches available today, we made an attempt to perform similar analysis using the ambient pressure dataset published by Hill (Hill, 1979). Those data were used as an input for a full multipole model refinement, although the quality of those results turned out to be quite limited. As a comparison benchmark, we also conducted X-ray measurements on diaspore at ambient pressure with our laboratory diffractometer.

We also performed a multipole model refinement for δ-AlOOH, using a published set of experimental XRD data by Komatsu *et al.* (2006). The data from the crystallographic information file deposited with that paper was used as a starting point to conduct multipole model refinement in the same way as it was conducted for our experimental data for the α-AlOOH phase. In addition optimisation of the δ-AlOOH structure with *CRYSTAL17* and calculations of dynamical structure factors ($\tilde{F}_{hkl}$) allowed us to obtain a theoretical density distribution. As a result, for both α and δ phases, we were able to obtain charge-density distributions on the basis of experimental data and theoretical calculations. Using these results, we attempted to compare the α and δ phases from the point of view of electron density distribution.

Describing a 3D structure with the use of polyhedra is just a convenient simplification. When one considers differences in electron density distribution, it is more beneficial to compare the shapes of atomic basins rather than the geometry of coordination polyhedra. Hence, in this study, we are using atomic basins rather than classic polyhedra to describe both investigated phases of AlOOH.

Experimental

Experimental quantitative charge-density studies

Aspherical modelling allows up to 32 additional parameters per atom, compared to routine refinements (Hansen and Coppens, 1978; Coppens *et al.*, 1979; Coppens and Coppens, 1997). The independent atom model (IAM) refines only 9 parameters, i.e. positions and atomic displacement parameters (ADPs), related to atomic thermal vibrations. However, a high resolution is

https://doi.org/10.1180/mgm.2024.22 Published online by Cambridge University Press

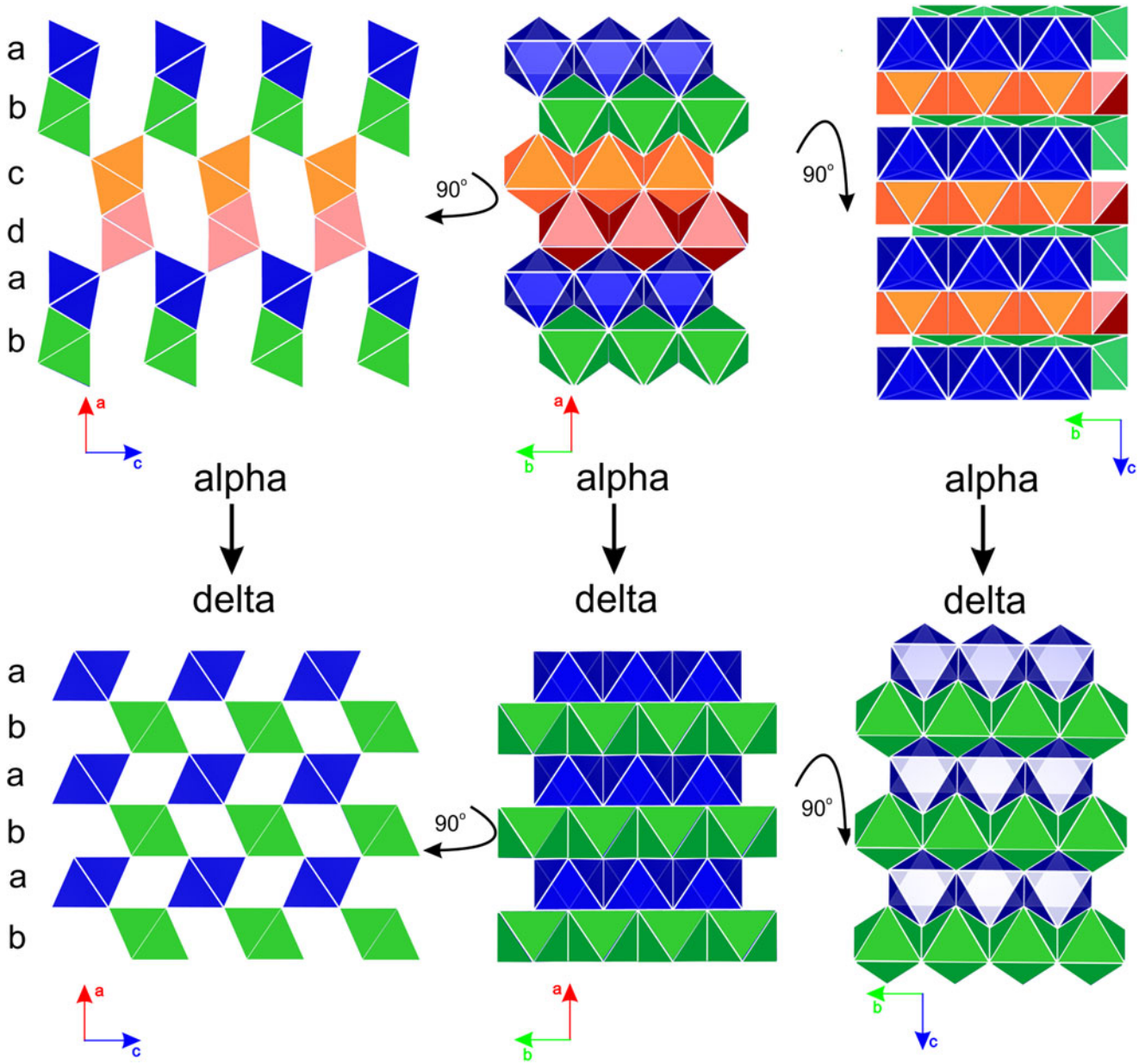

Figure 2. Structures of the α-AlOOH and δ-AlOOH phases with AlO_6 octahedra. Particular a, b, c and d chains of AlO_6 octahedra are depicted by different colours: blue, green, orange and pink, respectively. Crystal structures are drawn using *Vesta* (Momma and Izumi, 2011).

necessary to secure a sufficient observation/parameter ratio and to properly deconvolute the valence electron density from the thermal motions of atoms. High-resolution reflections are strongly associated with nuclear positions and with ADPs. The valence electron density contributes mostly to the low-angle diffraction reflections. The data set should be sufficiently complete to avoid systematic effects in the refinement – ideally 100% complete to a resolution higher that $\sin\theta/\lambda = 1$. Both accurate and precise measurements of the reflection intensities are needed to minimise systematic effects such as sample absorption, extinction and, very importantly, absorption by the apparatus itself, namely the diamonds and the metal gasket (Gajda *et al.*, 2020, 2022; Stachowicz *et al.*, 2023). Furthermore, the contribution of valence electrons to the total reflection intensity never exceeds a few percent, which reinforces the need for very accurate intensity measurements. Apart from accurate data correction, modern area-detector technologies offer the possibility to improve measurement precision by repeated collection of the same intensities (redundancy) (Sanjuan-Szklarz *et al.*, 2020).

The most common, aspherical quantitative model of experimental charge density is based on a finite spherical harmonic expansion of the electronic part of the charge distribution about each atomic centre, called a pseudo-atom. In the formalism of Hansen and Coppens (Hansen and Coppens, 1978; Coppens *et al.*, 1979) the pseudo-atom electron density is defined as:

$$\rho(\boldsymbol{r}) = \rho_c(r) + P_v\kappa^3\rho_v(\kappa r) + \sum_{l=0}^{l_{max}} \kappa'^3 R_l(\kappa' r) \sum_{m=0}^{l} P_{lm\pm}\, d_{lm\pm}\,(\theta, \varphi)$$

where $\rho_c(r)$ and $\rho_v(r)$ are spherical core and valence densities, respectively. The third term contains the sum of the angular

https://doi.org/10.1180/mgm.2024.22 Published online by Cambridge University Press

functions $d_{lm\pm}(\theta,\phi)$ to take into account the aspherical deformations. The angular functions $d_{lm\pm}(\theta,\phi)$ are real spherical harmonic functions. Coefficients P_v and $P_{lm\pm}$ are populations for the valence and deformation density multipoles, respectively. κ and κ' are scaling parameters introduced to make the valence and deformation densities expand or contract. In the Hansen–Coppens formalism, P_v, $P_{lm\pm}$, κ and κ' are refinable parameters together with the atomic coordinates and thermal coefficients. Least-squares refinements were performed against the measured intensities of reflections (i.e. $F^2(hkl)$) obtained by single-crystal X-ray diffraction. This requires a data resolution of 0.50 Å and 100% data completeness. Starting atomic coordinates and anisotropic displacement parameters are taken from the ordinary spherical refinement stage and freely refined. Each atom was assigned core and spherical-valence scattering factors derived from the Su and Coppens (1997) wavefunctions. A single-ζ Slater-type radial function multiplied by density-normalised spherical harmonics was used for describing the valence deformation terms. The multipole expansion was truncated at the hexadecapole level for Al and O atoms.

Once an aspherical atomic electron density ρ(r) was defined, then it could be used to obtain aspherical atomic form factors and aspherical structural factors for a given crystal.

In AIM theory (Bader, 1994; Popelier, 1996), a many electron system is separated into subsystems (ionic basins) by zero-flux surfaces (ZFSs). Any point on this surface satisfies the equation $\mathbf{n}\bullet\nabla\rho(\mathbf{r}) = 0$, where $\nabla\rho(\mathbf{r})$ is the gradient vector field of the electron density, **r** is a point on the zero-flux surface that separates two fragments, and **n** is the vector normal to the surface at that point. Further analysis of the gradient vector field of electron density results in localisation of the extremes of the electron density by finding critical points (CP) at which $\nabla\rho(\mathbf{r}_{CP}) = 0$. Particularly useful are bond critical points − the weakest points in bonds which define their properties. Integrating properties over ionic basins is one of the cornerstones of AIM theory because it yields valuable information such as the integrated charges, the volumes of atoms/ions, their energies, and electronic populations as well as higher multiple moments and polarisabilities (Angyan *et al.*, 1994).

Space-group setting

On the basis of powder-diffraction results, the δ-AlOOH phase structure of diaspore was first proposed as space group $P2_1nm$ (Suzuki *et al.*, 2000). Three space groups were proposed as stable structures from first principle calculations *Pnnm*, $P2_1nm$ and $Pn2_1m$ (Tsuchiya *et al.*, 2002). Finally, a single-crystal X-ray data collection led to the $P2_1nm$ space group (Komatsu *et al.*, 2006). Again, this is a non-standard setting of the space group. However in this paper, we describe α-ALOOH with the use of the standard setting *Pnma*. To be consistent, we used the standard setting of $Pmn2_1$ for the lower symmetry phase of diaspore. This setting is convenient to compare this structure with the *Pnma* structure. As described by Komatsu and co-workers (Komatsu *et al.*, 2006), a phase transition from the α to δ phase was possible at quite severe conditions, 18 GPa and 1273 K for 10 hrs. Generally, it is expected that HP causes shrinking of the unit cell and transformation to a crystal of higher symmetry. In our case the *Z* number changed from 4 in the alpha phase, to 2 in the delta phase. The equivalent volume/density difference between the two phases at ambient pressure is ca. 4.6%. The delta phase indeed has a lower volume and higher density.

Data quality

The primary goal of this paper is to compare electron density distribution in the crystal structure of the α and δ phase of AlOOH. As current experimental and literature data originated from different sources (different radiation sources) and were collected under different conditions (ambient or non-ambient pressure) the differences in the quality of these data sets are notable. This fact should be taken into consideration when comparing these results. The most basic parameters of particular data sets such as resolution, the number of measured reflections, total completeness, wavelength and pressure conditions are presented in Table 1.

The oldest literature data set, which was in fact the inspiration for the current investigation, was an attempt to refine the electron density distribution in diaspore conducted by Hill (1979). Although the resolution of this data set seems to be quite high, in fact, the completeness of data is rather poor. The completeness within the range typical for routine structural studies is close to 100% but varies between 50–70% for the high-resolution range. We have made an attempt to use this data set (the full list of reflections is available with the original publication) to refine the electron density according to the Hansen–Coppens multipole model (Hansen and Coppens, 1978; Coppens *et al.*, 1979). However, the results of refinement against the full *hkl* data set (791 reflections) are rather poor because the highest peaks and deepest holes in the residual density map are +1.78 and −1.95, respectively.

Our own experimental data set, which is the basis for the current considerations, was measured at the CRISTAL beamline of the SOLEIL synchrotron facility and was collected under high pressure. The experiment was conducted under pressure using a diamond-anvil cell, because we wanted to check if datasets collected in this way are suitable for obtaining the electron density distribution. If successful, further, more comprehensive, tests will be carried out. Ideally, the set of pressure points showing step by step how electron density changes as a function of pressure before and after a pressure triggered phase transition.

Although a single crystal was placed in the diamond-anvil cell, which causes a restriction of access to reciprocal space, due to the use of short-wavelength synchrotron X-ray radiation it was possible to collect X-ray diffraction data of a resolution comparable to the literature data (Hill, 1979) with even better completeness. This data set will be referred to as the SOLEIL experimental data.

As a benchmark we have also collected a dataset of diaspore at ambient pressure on our laboratory diffractometer (λ = 0.56087). This data will be referred to as the Lab. Diffract. Experiment. These data are our only experimental data which are, in practise, 100% complete.

The 4th experimental data set considered in this paper is literature data for the δ-AlOOH phase (Komatsu *et al.*, 2006). The crystallographic information file attached to this manuscript contains a list of all the measured intensities of reflections, allowing an attempt to refine the electron density for this structure according to the Hansen–Coppens multipole model (Hansen and Coppens, 1978; Coppens *et al.*, 1979). This data set was collected at the synchrotron facility (in Table 1 named 'δ-AlOOH experiment'). However, the beam wavelength was relatively long λ = 0.7007(1) Å. Only 262 reflections were measured which gave a completeness of only 62%. Such a poor resolution and completeness will affect the results of any refinement, especially of the multipole model of electron density refinement. Our analysis of the given list of reflections revealed that only a half of the potentially accessible reciprocal space was measured. Therefore to

https://doi.org/10.1180/mgm.2024.22 Published online by Cambridge University Press

Table 1. Quality of the data sets investigated.

	α-AlOOH Hill (1979) experiment	α-AlOOH SOLEIL experiment	α-AlOOH CRYSTAL	α-AlOOH Lab. Diffract. experiment	δ-AlOOH Komatsu *et al.* (2006) experiment	δ-AlOOH CRYSTAL
$\sin\theta/\lambda_{max}$ [Å^{-1}]	1.28	1.25	1.03	1.02	0.96	0.97
Unique reflections	791	753	568	584	262	485
Completeness [%]	76.95	79.35	100	99.8	62	100
λ [Å]	0.7093	0.4162	-	0.5609	0.7007	-
P [GPa]	ambient	2.5	-	ambient	ambient	-

improve the results, we decided to support the experimental data with the theoretical.

As the first step of preparing the input data set for the multipole refinement based on theoretical calculations, the crystal structure of δ-AlOOH (reflections from Komatsu *et al.*, 2006) was optimised in *CRYSTAL17* (Dovesi *et al.*, 2005, 2018). We used the *B3LYP* (Lee *et al.*, 1988; Becke, 1993) exchange–correlation function corrected for dispersion by Grimme's *D3* (Grimme *et al.*, 2010) correction in conjunction with the *pob-TZVP-rev2* basis sets (Vilela Oliveira *et al.*, 2019). Calculations were conducted for ambient pressure. Optimisation of the atomic position and cell volume was allowed. Convergence criterion on the root mean square of the gradient (TOLDEG = 0.00085), as well as on the displacement (TOLDEX = 0.0009), was also employed. The calculation grid had 75 radial points and maximum number of 974 angular points in the regions relevant for chemical bonding (XLGRID). The truncation criteria for bi-electronic integrals were adopted (TOLINTEG = 7 7 7 9 30). A Pack-Monkhorst/Gilat shrinking factor was also used (8 − shrinking factor in reciprocal space, 16 − shrinking factor for Gilat net). The convergence accelerator (BROYDEN) was also used. Fock matrices and KS matrices were mixed in a 50:50 ratio.

The dynamical structure factors ($\tilde{F}_{hkl}$) were calculated (Erba *et al.*, 2013). The list of structure factors was built in such a way that the resolution given in the experimental data was preserved and, additionally, not measured but potentially accessible reflections were added to the list. As a result, theoretical data which correspond to the experimental δ-AlOOH data set had a comparable resolution but completeness equal to 100% ('δ-AlOOH CRYSTAL17' in Table 1).

The theoretical data set corresponding to α-AlOOH (based on the SOLEIL experiment) was prepared similarly. In the case of the α-AlOOH data set, the theoretical list of reflections was cut slightly to obtain resolution and completeness comparable to the δ-AlOOH experimental data.

These prepared structure factors were used as the input data sets for multipole refinement which was carried out in the same way as the refinements of the experimental data sets. There are two major differences between the experimental and theoretical data sets which should be underlined here. Firstly, the experimental *hkl* file contains the experimentally measured reflection intensities ($I(hkl) \approx F(hkl)^2$) with their sample standard deviations. Secondly, whereas theoretical *hkl* files contain calculated dynamical structure factors ($\tilde{F}_{hkl}$) and because they are calculated, they have no sample standard deviations although they were used in the optimisation in the same form as the experimental values.

Data reduction

Data reduction for all the frames collected was performed using *CrysAlisPRO* software (CrysAlis Pro, 2014). Next, the structures were solved and refined with *ShelXS* (Sheldrick, 2008) and *ShelXL* (Sheldrick, 2015), respectively, within the *Olex2* suite (Dolomanov *et al.*, 2009). Then, the intensities for each of the measurements were merged using *Sortav* (Blessing, 1995) implemented in the *WinGX* program suite (Farrugia, 2012). The merged reflection intensity data sets were used subsequently as an input for the *XD2016* (Volkov *et al.*, 2016) program.

Parameters describing results of IAM refinement of only the experimental data (including literature data) are presented in Table 2. Table 3 presents results of multipole refinement conducted on the basis of experimental data as well as theoretical calculations. For all the datasets in Table 3 the same weighting scheme was used: $w2 = 1/[s^2(F_o^2)]$. Literature references indicate which original data were used as the starting point for refinement. The number of parameters determined in each refinement presented in Table 3 was slightly different. For α-AlOOH (theoretical data), it was possible to refine the κ and κ' parameters for both Al and O atoms. For α-AlOOH (SOLEIL experiment), κ' was not refined. For α-AlOOH (based on Hill's data), only κ for oxygen atoms was refined and the dipole parameter for hydrogen atom was not refined. In the case of both δ-AlOOH, the number of parameters was lower because for Al only the monopole was refined. The value of *S* (goodness of fit) for purely computational and for computationally augmented data was unreasonably high due to the fact that no uncertainty estimates for reflection intensities were available from the calculations, and standard deviations were arbitrarily set to unit values of sigma to fulfil the software requirements.

The CSD entries with deposition numbers 2298866–2298867 and 2307563–2307564 contain the supplementary crystallographic data for the α-AlOOH system investigated in this paper. This data can be obtained freely via http://www.ccdc.cam.ac.uk/data_request/cif, or by contacting data_request@ccdc.cam.ac.uk or the Cambridge Crystallographic Data Centre directly. The crystallographic information files have also been deposited with the Principal Editor of *Mineralogical Magazine* and are available as Supplementary material (see below)

Results and discussion

Phase comparison

The crystal structure of diaspore α-AlOOH is relatively simple. The crystal system is orthorhombic with four molecules within the unit cell. Two different mirror planes pass through each unit cell and all of the atoms are placed on these planes. As a result each atom is at a special position with the occupation factor equal to ½. In the asymmetric part of the unit cell, there are: one aluminium, one hydrogen atom, and two types of oxygen atoms (one of them is bonded with hydrogen and the other is not) (see Fig. 1). Each Al atom is surrounded by six oxygen atoms (three bonded with hydrogens and three not bonded). In fact,

https://doi.org/10.1180/mgm.2024.22 Published online by Cambridge University Press

Table 2. Selected crystal data for IAM refinements of AlOOH.

Data source	α-AlOOH SOLEIL experiment	α-AlOOH Lab. Diffract. experiment	α-AlOOH Hill (1979) experiment	δ-AlOOH Komatsu *et al.* (2006) experiment
a (Å)	9.3873(2)	9.42732(19)	9.4253(13)	4.222
b (Å)	2.83254(5)	2.84534(6)	2.8452(3)	2.831
c (Å)	4.36908(19)	4.40158(9)	4.4007(6)	4.713
V (Å^3)	116.17(1)	118.07(1)	118.01(3)	56.3
Z, *F*(000)	4, 120	4, 120	4, 120	2, 60
D_x (Mg m^{-3})	3.430	3.375	3.376	3.536
μ (mm^{-1})	0.25	0.51	1.00	1.01
Crystal size (mm)	0.15×0.1×0.1	0.21×0.15×0.08	0.11×0.11×0.06	0.04×0.04×0.04
Absorption correction	Multi-scan	Gaussian	Gaussian	none
Measured reflections	6404	5157	791	1633
Independent reflections	753	584	791	262
Observed reflections	717	542	773	262
R_{int}	0.055	0.033	*no data*	0.034
θ values (°)	θ_{max} = 31.3, θ_{min} = 2.5	θ_{max} = 35.0, θ_{min} = 4.0	θ_{max} = 65.1, θ_{min} = 4.3	θ_{max} = 42.5, θ_{min} = 4.8
Range of *h*, *k*, *l*	*h* = −16→22 *k* = −7→4 *l* = −6→8	*h* = 19→19 *k* = −5→5 *l* = −8→8	*h* = 0→10 *k* = 0→12 *l* = 0→7	*h* = 0→9 *k* = 0→8 *l* = 0→5
Refinement on, parameters, reflections	F^2, 22, 753	F^2, 23, 584	F^2, 23, 791	F^2, 22, 262
$R[F^2 > 2\sigma(F^2)]$, $wR(F^2)$, *S*	0.025, 0.069, 1.14	0.019, 0.050, 1.18	0.054, 0.113, 1.36	0.014, 0.041, 1.31
Weighting scheme	$w = 1/[\sigma^2(F_o^2) + (0.0385P)^2 + 0.0041P]$ where $P = (F_o^2 + 2F_c^2)/3$	$w = 1/[\sigma^2(F_o^2) + (0.0177P)^2 + 0.0341P]$ where $P = (F_o^2 + 2F_c^2)/3$	$w = 1/[\sigma^2(F_o^2) + (0.0155P)^2 + 0.3672P]$ where $P = (F_o^2 + 2F_c^2)/3$	$w = 1/[\sigma^2(F_o^2) + (0.0175P)^2 + 0.0123P]$ where $P = (F_o^2 + 2F_c^2)/3$
$(\Delta/\sigma)_{max}$	0.001	0.001	0.001	0.001
Largest diff. peak/hole (*e* Å^{-3})	0.47, −0.37	0.39, −0.35	1.18, −0.94	0.34, −0.35

the most common structural element of the crystal structure is an AlO_6 octahedron. Octahedra are arranged in a specific way (see Fig. 2).

In the α-AlOOH structure, the edge-sharing AlO_6 octahedra are organised in chains along the y-direction. Within such a chain, the octahedra have the same orientation. Each chain of octahedra is connected with three other chains, with one of them sharing edges, and two others sharing vertices. Tunnels in the crystal structure along the z-axis are formed between the chains connected in this manner.

To simplify this description, we can distinguish four repeating types of chains within the diaspore structure (marked as a to d and depicted with different colours in Fig. 2. Some voids between polyhedra are clearly visible along the [010] direction and are filled by the O–H···O hydrogen bonds, omitted for clarity in Fig. 2. At ambient temperature, the pressure of 18 GPa is not high enough to trigger the phase transition by itself, due to the high-activation barrier. The sample must also be heated for many hours at a temperature close to 1000°C, which illustrates that a significant amount of energy must be delivered to the system to break the existing connections and rearrange the AlO_6 blocks.

In the δ phase, the atomic arrangement after phase transition seems to be very similar to that observed in the α-AlOOH phase. Four atoms in the asymmetric unit are located on a mirror plane. The Al cation at the centre of the octahedral site is coordinated by two types of oxygen atoms. In the δ-phase, the oxygen atoms are placed at the intersection of mirror and glide planes. As the oxygen atoms in the δ-phase have fewer degrees of freedom, it is expected that the deformation of octahedra could be smaller. When the structure is depicted in the form of AlO_6 octahedra, it is easy to understand how it has changed in comparison with the α-AlOOH phase (see Fig. 2). The structure of the δ-phase is simplified because instead of four repeating chains of AlO_6 octahedra in α-AlOOH there are only two of them.

In Fig. 3, one can clearly see that a schematic concept of the polyhedra does not necessarily correspond directly to the shapes and orientations of the atomic basins. First, in the polyhedral representation, ligand atoms are placed at the vertices of the polyhedra, whereas in the basins representation of the ligands are

Table 3. Selected data describing results of multipole refinement of electron density.

	α-AlOOH SOLEIL experiment	α-AlOOH CRYST.17	α-AlOOH Lab. Diffr. experiment	α-AlOOH Hill (1979) experiment	δ-AlOOH Komatsu *et al.* (2006) experiment	δ-AlOOH CRYST.17
Refinement on, parameters, reflections	F^2, 71, 669	F^2, 73, 566	F^2, 66, 508	F^2, 69, 752	F^2, 59, 262	F^2, 59, 485
R[F2>2σ(F2)]	0.0338	0.003	0.018	0.1073	0.0247	0.0105
R(all)	0.0349	0.003	0.021	0.1079	0.0247	0.0105
w*R*[F2>2σ(F2)]	0.0436	0.005	0.042	0.1227 10.1635	0.0232	0.0159
S	1.0241	22.552	1.207		2.3610	53.5016
Largest diff. peak/hole (e^- Å^{-3})	0.570	0.084	0.280	1.784	0.304	0.177
	−0.406	−0.089	−0.465	−1.946	−0.390	−0.132

https://doi.org/10.1180/mgm.2024.22 Published online by Cambridge University Press

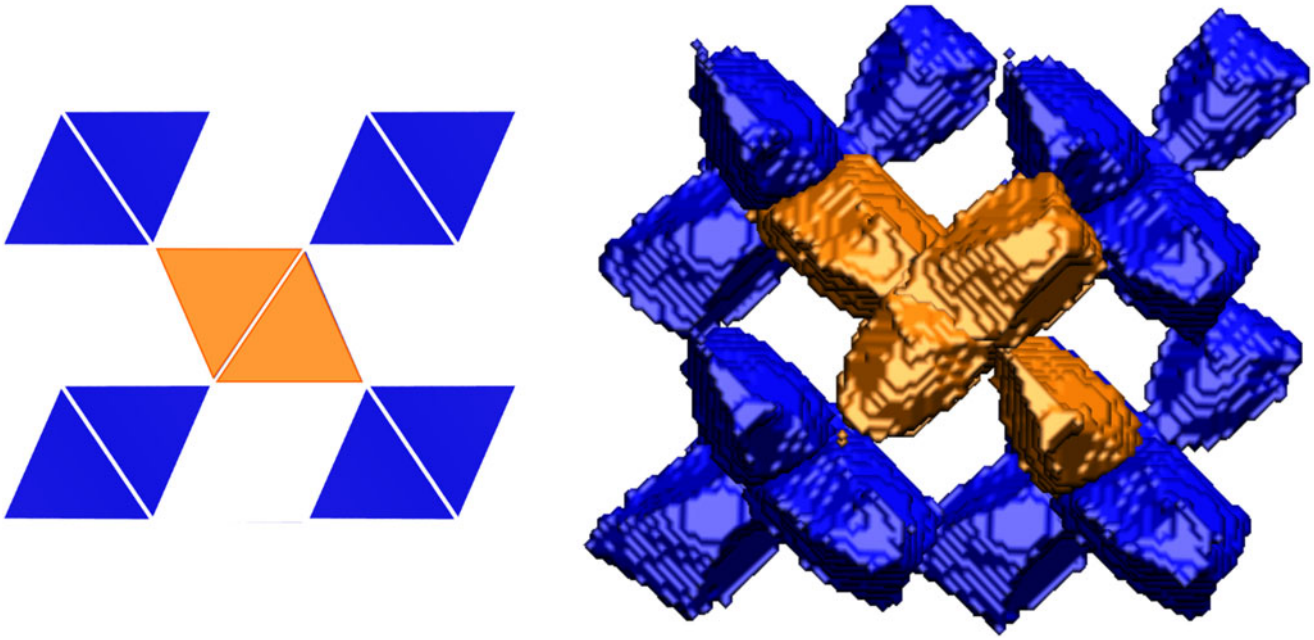

Figure 3. The δ-ALOOH phase. Comparison of polyhedra and atomic basins. View along the [010] axis.

located inside the atomic basins. For that reason, all the atomic basins which belong to the central polyhedron in Fig. 3 are coloured orange. Second, the volumes of polyhedra have nothing in common with the volumes of corresponding atomic basins. In the case of atomic basins, the electron density which belongs to a particular atom is inside the 3D boundaries. For polyhedra, their boundaries have, in fact, no physical meaning.

Atomic basins

Atomic basins are a good representation of the distribution and partition of electron density. They can be compared within groups of corresponding to typical structural elements, for example, the AlO_6 blocks in the structure of AlOOH. Examples of such aggregates for both phases are depicted in Fig. 4. To distinguish the existence of two types of oxygen atoms, the first one with bonds to hydrogens and the second one with the non-bonding interactions, particular basins are coloured in purple and orange, respectively. The same colouring scheme is used also in the case of the δ-AlOOH phase.

Arrangement of particular atomic basins is worth consideration in the context of their closest surroundings. Atomic basins describing the AlO_6 octahedron in the crystal structure of the α-AlOOH phase are presented in Fig. 5. The α-phase is relatively densely packed. Atomic basins belonging to the oxygen atoms cover the Al basin completely from each side. The basins should fill in the space of the unit cell completely (taking hydrogens into account). The phase transition causes rearrangement of the building blocks (see Fig. 6). The higher pressure δ-AlOOH phase results in a lower symmetry structure. The oxygen atomic basins have much more irregular shape than those in the α-phase. The basins of the type 1 oxygen atoms (bonding with hydrogen atoms, purple shapes) are smaller and their shape is slimmer in comparison with bulky type 2 oxygen basins (orange shapes). Atomic basins describing the AlO_6 group in the crystal structure of the δ-AlOOH phase are presented in Fig. 6.

As a consequence of rearrangement of electron density distribution (EDD), the atomic positions are affected and phase transition can occur. Such rearrangement of EDD can be visualised by maps of total electron density (see Fig. 7, second row). One can see that redistribution of EDD is significant and results in unquestionable phase transition. In δ-AlOOH, all atoms are placed at special positions on the mirror plane (the same situation as with α-AlOOH). That is why it is convenient to choose such a plane to compare molecular arrangements in both space groups.

At the first glance, it seems that transition from *Pnma* to $Pnm2_1$ results only in a twofold screw axes along the z-direction instead of the ***a*** glide plane perpendicular to the z-axis. In fact, we are losing more symmetry elements. As a result of the phase transition from the α-AlOOH to δ-AlOOH phase, the ***a*** glides perpendicular to the z-axis disappear as well as the twofold screw axes along the x and y axes.

However, such two-dimensional maps show only some small fragments of the structure and the 3D visualisations (i.e. atomic basins) could be much more convenient in some aspects).

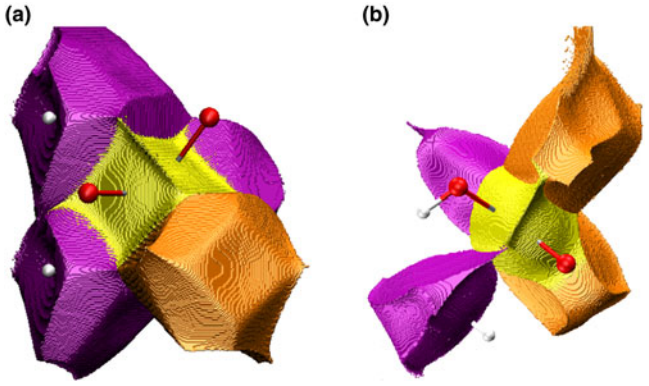

Figure 4. Selected atomic basins forming the AlO_6 octahedra of in the phases α-AlOOH (a) and δ-AlOOH (b). Yellow basin = aluminium atom; purple basins = oxygen atoms bonded with hydrogen atoms; orange basins = oxygen atoms which are not bonded with hydrogen atoms.

https://doi.org/10.1180/mgm.2024.22 Published online by Cambridge University Press

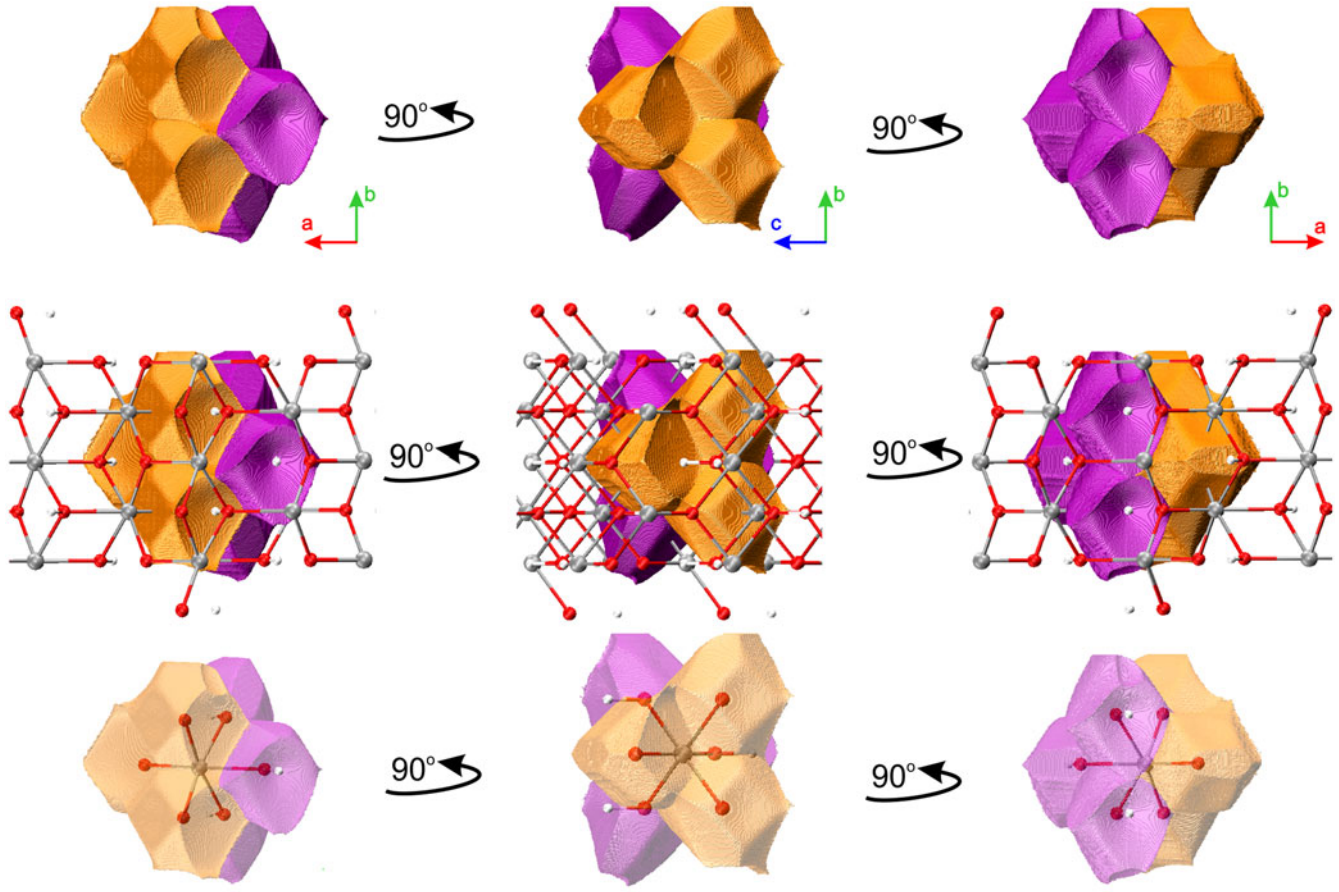

Figure 5. Atomic basins of AlO_6 octahedra in the α-AlOOH phase. Purple basins = oxygen atoms bonded with hydrogen atoms; orange basins = oxygen atoms which are not bonded with hydrogen atoms; aluminium basins are not visible.

Information about the fractional atomic coordinates and U_{eq} values for both types of refined structures, α-AlOOH and δ-AlOOH are presented in Table 4.

Integrated atomic values

Integrated atomic charges and volumes are included in the Tables 5 and 6, respectively. The tables only contain results for α-AlOOH because basin integration for δ-AlOOH was not successful. One of the reasons could be the relatively poor data for δ-AlOOH.

In general, integrated atomic charges and volumes are important indicators of the quality of the multipole refinement. The refined molecule (or pair of anion and cation) should be neutral and the sum of all the atomic basins (within unit cell) together should be equal to the volume of the unit cell. Only minimal discrepancies can be allowed.

For charges, the Hill's data leads to relatively significant underestimation of the charge on Al(1) (ca. +1.47 e^-) compared to the modern ambient experimental (2.29 e^-) and theoretical data (2.57 e^-), as well as the 2.5 GPa synchrotron results (2.33 e^-). In addition, the literature charge value for O(2) is over two times smaller than that calculated for datasets collected in this work. However, literature data indicates a neutral molecule, whereas our calculations show small deviations from 0. Additionally, due to the specific calculation procedure our data are not accompanied by defined systematic error. Neither the experimental nor theoretical total ionic charges take formal values.

For the atomic volumes (Table 6), there was quite good agreement between the experimental atomic volumes calculated on the basis of the experimental data from SOLEIL and the results obtained by applying CRYSTAL17. The only exception was the atomic volume of H(1) which was far smaller when the experimental data from SOLEIL were used (1.12 $Å^3$) compared to 3.19 $Å^3$ for the theoretical data from CRYSTAL17. In each case the sum of all atomic basins (within unit cell) is very close to the volume of the whole unit cell.

Bond critical points

Selected parameters at bond critical points (BCP) such as electron density and Laplacian values are given in Table 7. In the case of bond-critical points, the spread of results was bigger than that of the integrated atomic values. It was not clear why the BCP was not found for the O(1)–H(1) bond in α-AlOOH (CRYSTAL17) or δ-AlOOH (experimental data). In our opinion it might have been due to the limited quality of the data.

Especially interesting was comparison of the Laplacian values. According to the theory of atoms in molecules (AIM) there are shared and closed-shell interactions (Bader, 1994, 2006; Zhang *et al.*, 2009). The shared interaction has a large value for charge density and a negative Laplacian value at the BCP, whereas the closed-shell interaction has a small charge-density value and a positive Laplacian value at the BCP. In this way, the charge density and Laplacian values at the BCP can characterise the nature of the bonding.

https://doi.org/10.1180/mgm.2024.22 Published online by Cambridge University Press

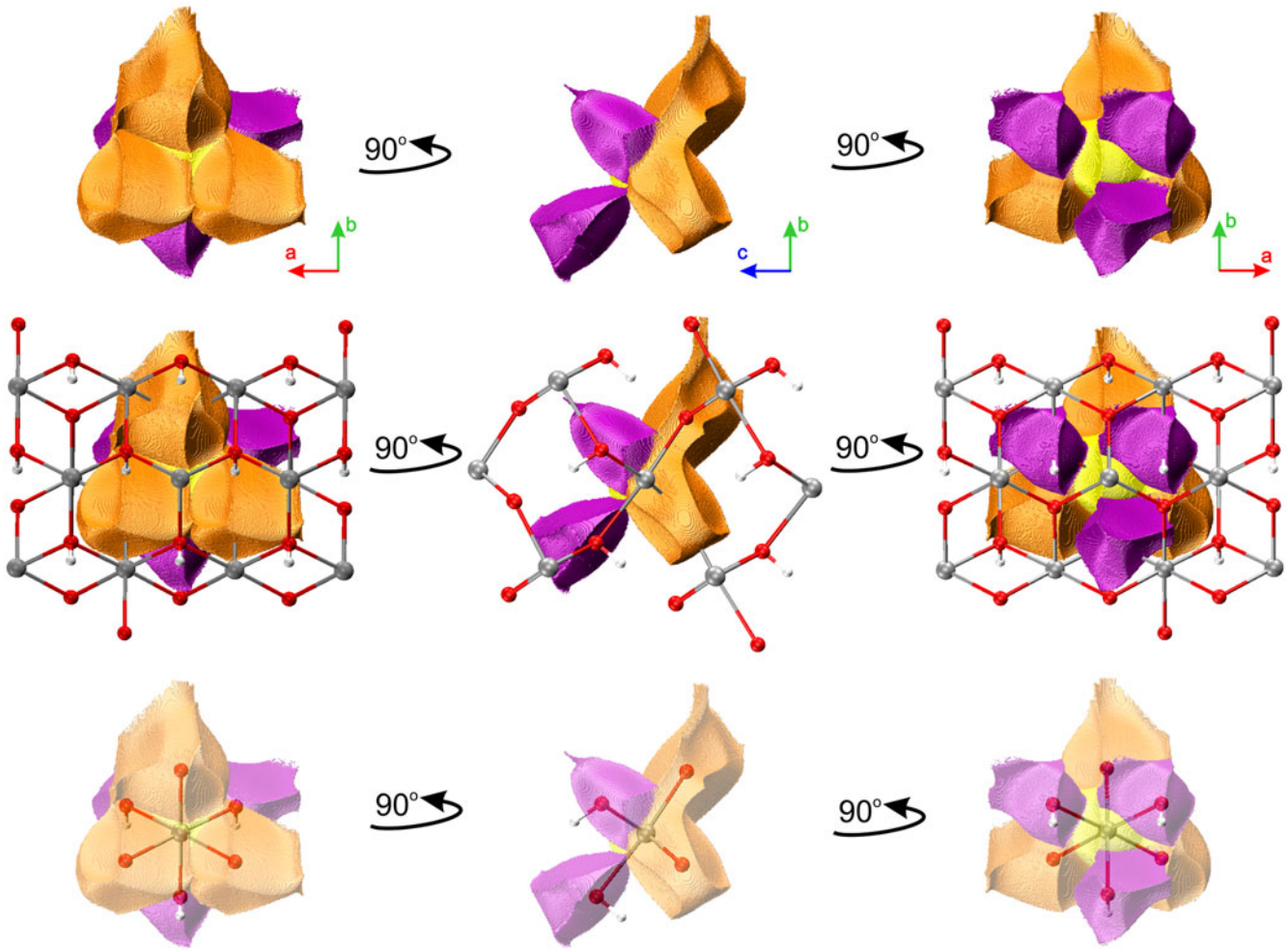

Figure 6. Atomic basins of the AlO_6 group of atoms in the δ-AlOOH phase. Yellow basin = aluminium atom; purple basins = oxygen atoms bonded with hydrogen atoms; orange basins = oxygen atoms which are not bonded with hydrogen atoms.

Positive Laplacian values usually indicates ionic bonding whereas negative Laplacian values indicate covalent bonding. In the case of positive Laplacian values there is another possible explanation: a charge-shift bond where the covalent term is repulsive rather than attractive. In Table 7 we see that O–H bonds are clearly shared interactions (covalent bonds), because they have relatively high charge-density values and negative Laplacian values, as expected. However, these results are no longer so clear in the case of the Al–O interactions. For both phases α and δ results correspond with synchrotron experiments and their theoretical benchmarks show positive Laplacian values (closed-shell interaction). The results of our experiments conducted on our laboratory diffractometer shows that the Laplacian values of the Al–O bonds are no longer clearly positive but rather gently negative. Taking into account that the dataset from our laboratory diffractometer is the only one which is 100% complete it raises the question how much such a sensitive parameter such as the Laplacian (second derivative of charge density) could be affected by low data completeness. We think that this might be such a case.

Al–O bonds and distortion of AlO_6 octahedra.

Bond length values and polyhedral distortion parameters are in Tables 8 and 9, respectively. For the bond lengths, there was a good agreement between the final results from our laboratory experiments (diffractometer with Ag X-ray source) with Hill's results. The Al(1)–O(1) bond lengths in δ-AlOOH were slightly shorter than in α-AlOOH and the reverse was true for the Al(1)–O(2) bond length (see Table 8). In general, the bond lengths agreed very well. The largest differences were for the valence angles, for example, when Hill's data were compared with the SOLEIL data set, the differences were as large as 8.19(6)° for the O(1)–Al(1)–O(2) or O(1)–Al(1)–O(2) valence angles.

The parameter $d_{\text{mean,}}$ used in Table 9, refers to the average Al–O distance in the AlO_6 octahedron. Other parameters such as ζ and Σ describe the stretching and angular distortions, respectively. Parameters ζ, Δ and Σ are defined as follows:

$$\zeta = \sum_{i=1}^{6} |d_i - d_{mean}|$$

$$\Delta = \frac{1}{6}\sum_{i=1}^{6}\left(\frac{d_i - d_{mean}}{d_{mean}}\right)^2$$

$$\sum = \sum_{i=1}^{12} |90 - \phi_i|$$

https://doi.org/10.1180/mgm.2024.22 Published online by Cambridge University Press

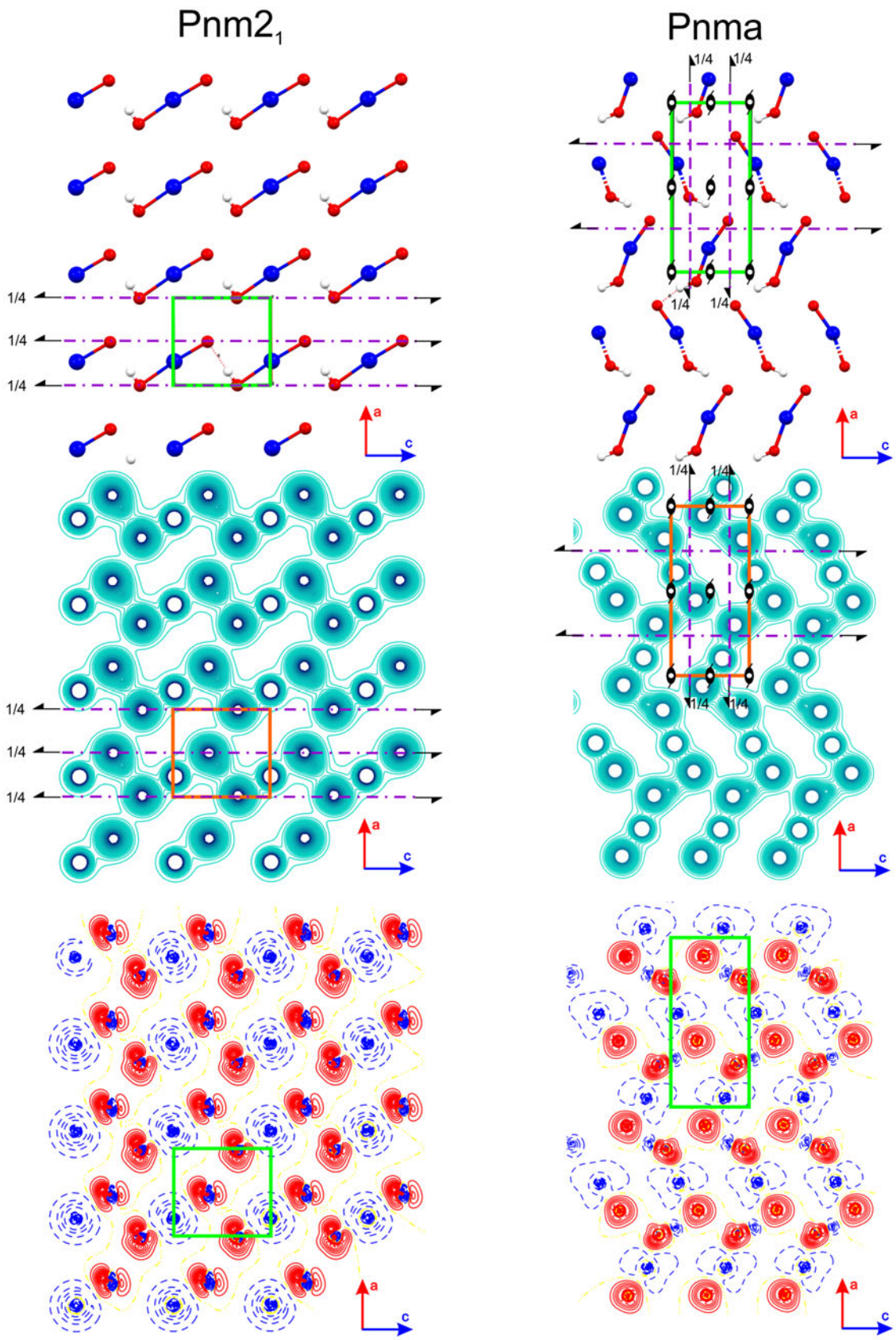

Figure 7. Comparison of the atomic arrangements in the α-AlOOH and δ-AlOOH phases. The 1st row: atomic positions and symmetry elements with unit cells defined. The 2nd row: unit cell with symmetry elements with the total charge-density distributions in the background. The 3rd row: deformation electron density distributions – views along the y-axis.

https://doi.org/10.1180/mgm.2024.22 Published online by Cambridge University Press

Table 4. Fractional atomic coordinates and U_{eq} values after multipole refinement.

Atom	x/a	y/b	z/c	U_{eq}
α-AlOOH SOLEIL experiment				
Al(1)	0.143849(19)	¾	0.45502(6)	0.004
O(1)	0.05343(4)	¼	0.69898(12)	0.005
O(2)	0.19853(4)	¼	0.21061(12)	0.004
H(1)	0.092(4)	¼	0.910(10)	0.018
α-AlOOH CRYSTAL17				
Al(1)	0.142094(2)	¾	0.451467(6)	0.009
O(1)	0.055074(7)	¼	0.699167(16)	0.011
O(2)	0.196118(7)	¼	0.201142(15)	0.011
H(1)	0.0916(5)	¼	0.9136(15)	0.100
α-AlOOH Lab. Diffr. experiment				
Al(1)	0.14456(2)	¾	0.45517(4)	0.004
O(1)	0.05340(8)	¼	0.69790(18)	0.005
O(2)	0.19910(8)	¼	0.21276(16)	0.005
H(1)	0.083(3)	¼	0.868(6)	0.002
δ-AlOOH Komatsu *et al.* (2006) experiment				
Al(1)	0.274525	0	−0.00031(7)	0.003
O(1)	−0.000853	0	0.35436(9)	0.004
O(2)	0.49849	0	−0.34174(9)	0.004
H(1)	0.154958	0	0.456(6)	0.003
δ-AlOOH CRYSTAL17				
Al(1)	0.271806	0	0.00783(11)	0.006
O(1)	0.002344	0	−0.34706(7)	0.009
O(2)	0.495947	−0.003(10)	0.35244(7)	0.008
H(1)	0.202539	0	-0.460(6)	0.014

Table 5. Net atomic charge in the α-AlOOH phase.

Atom	α-AlOOH SOLEIL experiment	α-AlOOH CRYSTAL17	α-AlOOH Lab. Diffr. experiment	α-AlOOH Hill (1979) experiment
Al(1)	+2.33	+2.57	+2.29	+1.47(26)
O(1)	−1.47	−0.95	−1.07	−1.08(16)
O(2)	−1.26	−1.43	−1.66	−0.59(13)
H(1)	+0.70	-0.08	+0.53	+0.20(5)
Total per molecule	+0.30	+0.11	+0.09	0

Table 6. Integrated atomic volumes in the α-AlOOH phase.

Atomic volume [Å^3]	α-AlOOH SOLEIL experiment	α-AlOOH CRYSTAL17	α-AlOOH Lab. Diffr. experiment
Al(1)	3.49	3.29	3.67
O(1)	12.48	10.52	11.69
O(2)	11.76	11.74	12.33
H(1)	1.12	3.19	1.72
Total	115.40 (116.17*)	114.96 (115.03**)	117.64 (118.07*)

* volume of the experimental unit cell; **volume of the unit cell calculated theoretically

Parameter ζ is the average of the sum of the deviation of 6 unique Al–O bond lengths around the central Al atom (d_i) from the average value (d_{mean}). Parameter Δ is the octahedral distortion parameter (Lufaso and Woodward, 2004). Parameter Σ is the sum of the deviation of 12 unique cis O–Al–O angles (ϕ_i) from 90°. All the mentioned parameters were calculated with use of *OctaDist* (Ketkaew *et al.*, 2021).

Hydrogen bonds

Several scientific papers considered the issue of symmetrisation of hydrogen bonds in the structure of δ-AlOOH. (Sano-Furukawa *et al.*, 2008, 2009, 2018; Cortona, 2017; Kang *et al.*, 2017; Pillai *et al.*, 2018; Trybel *et al.*, 2021; Luo *et al.*, 2022) At ambient pressure, the hydrogen atom in the O(1)–H···O(2) hydrogen bond is located much closer to the O(1) donor atom than to the O(2) acceptor atom, and the potential energy surface for the hydrogen has a double well shape. However, pressure significantly changes this configuration. The energy barrier separating the two minima first becomes shallow enough that the hydrogen atom becomes disordered between two alternative sites, and eventually assumes a symmetrical position midway between O(1) and O(2), resulting in two subtle phase transitions. The structures investigated in our paper were measured (calculated) either at ambient conditions or at relatively low pressure, which is why such phenomena were not observed. The bond length between hydrogen and heavy atoms determined on the basis of X-ray measurements were usually shortened in comparison to neutron data. This is because of the shift of electron density in this bond towards the heavy atom and because of thermal motion of the H-atom which shortened the X–H bond length. The experimental data for α-AlOOH (Hill, 1979) reported a 0.9886(8) Å O–H distance, whereas experimental data for δ-AlOOH (Komatsu *et al.*, 2006) reported an O–H distance equal to 0.81(4) Å. In the case of our multipolar refinement, when the data were incomplete, we decided to fix O–H bond length and not refine it. In the case of 100% complete data from a diffractometer (α-AlOOH Lab. Diffr. Experiment), the O–H bond was fully refined and determined as equal to 0.88(3) Å. This value was of course shorter than those obtained on the basis of neutron measurements but is typical for X-ray measurements.

Conclusions

Comparison of data sets which were collected under different circumstances and have different qualities is quite challenging, especially when a particular set of data has lower-than-expected completeness. However, even though some details seemed not to be determined precisely, it was still possible to focus on general trends. The α–δ phase transitions in AlOOH were triggered by

Table 7. Charge density (1st row) and Laplacian (2nd row) at Bond Critical Points (3, −1).

Bond	α-AlOOH SOLEIL experiment	α-AlOOH CRYSTAL17	α-AlOOH Lab. Diffr. experiment	δ-AlOOH Komatsu *et al.* (2006) experiment	δ-AlOOH CRYSTAL17
Al(1)–O(1)	0.26(3)	0.364(2)	0.538(12)	0.357(6)	0.496(3)
	4.69(6)	8.444(4)	−0.916(32)	10.013(6)	2.712(2)
Al(1)–O(2)	0.74(2)	0.450(3)	0.790(13)	0.27(4)	0.207(4)
	9.66(3)	11.018(3)	−0.095(32)	5.69(1)	10.902(4)
O(1)–H(1)	2.18(4)	–	2.351(35)	-	2.9(7)
	−39.6(2)		−54.662(102)		−25.917(NA)

https://doi.org/10.1180/mgm.2024.22 Published online by Cambridge University Press

Table 8. Al–O bonds and O–Al–O angles.

	α-AlOOH SOLEIL experiment	α-AlOOH Hill (1979) experiment	α-AlOOH CRYSTAL17	α-AlOOH Lab. Diffr. experiment	δ-AlOOH Komatsu *et al.* (2006) experiment	δ-AlOOH CRYSTAL17
Al(1)–O(1)	1.9653(4)	1.9798(17)	1.96101(7)	1.9758(5)	1.8664(6)	1.8697(7)
Al(1)–O(1)$^{(i)}$	1.9703(4)	1.9749(10)	1.95481(5)	1.9841(8)	1.8658(3)	1.86(2)
Al(1)–O(2)	1.8465(3)	1.8581(15)	1.86349(7)	1.8512(5)	2.0361(5)	2.0113(6)
Al(1)–O(2)$^{(ii)}$	1.8538(5)	1.8528(8)	1.85385(5)	1.8595(8)	1.9516(2)	1.9421(3)
O(1)–Al(1)–O(1)$^{(i)}$	77.25(2)	76.92(5)	77.836(3)	76.97(3)	94.88(1)	94.3(6)
O(1)–Al(1)–O(2)	170.55(2)	162.36(6)	163.960(3)	170.35(3)	175.62(2)	176.01(6)
O(1)–Al(1)–O(2)$^{(ii)}$	83.17(1)	93.78(6)	93.603(2)	83.06(2)	89.85(2)	89.4(6)

α: (i) $-x$, ½+y, 1–z; (ii) ½–x, 1–y, –½+z; δ: (i) 1–x, ½–y, ½+z; (ii) $-x$, ½–y, –½+z

Table 9. Octahedral distortion parameters

	α-AlOOH SOLEIL experiment	α-AlOOH Hill (1979) experiment	α-AlOOH CRYSTAL17	α-AlOOH Lab. Diffr. experiment	δ-AlOOH Komatsu *et al.* (2006) experiment	δ-AlOOH CRYSTAL17
d_{mean} [Å]	1.908	1.916	1.907	1.916	1.923	1.913
ζ [Å]	0.353	0.366	0.299	0.374	0.341	0.314
Δ	0.000954	0.001017	0.000689	0.001062	0.001089	0.000898
Σ [°]	75.50	76.92	73.27	76.83	43.73	41.47

Note – the symbols are described in the text.

high pressure and temperature, and caused significant reorganisation of the distribution of electron density. As a consequence, the crystal symmetry was lowered, significant reduction of the unit cell took place, and the basic AlO_6 building blocks of the structure were rearranged.

This study demonstrates that when we compare currently collected datasets with those collected thirty or forty years ago we face problems. Issues caused by factors such as differences in hardware (detectors) and software (for example different treatment of weak reflections) quality. That is why straightforward comparison of older and current datasets is not always possible.

However, comparing the multiple data sets examined in this paper together (including historical data), we found common features, and showed that augmenting experimental data with computational results can help even incomplete data to reveal important information. Although the high-pressure high-resolution data of α-AlOOH are not 100% complete, they still clearly correspond with previously collected data and allow one to make suppositions about how phase transitions affect crystal structures.

Acknowledgements. Financial support for this work provided by the National Science Centre, Poland (OPUS grant No. UMO-2019/33/B/ST10/02671 awarded to KW) is gratefully acknowledged. This work was partly carried out at the Biological and Chemical Research Centre, University of Warsaw, established within the project co-financed by the European Union from the European Regional Development Fund under the Operational Programme Innovative Economy, 2007–2013. The work was accomplished at the TEAM TECH Core Facility for crystallographic and biophysical research to support the development of medicinal products sponsored by the Foundation for Polish Science (FNP). The synchrotron radiation experiments were performed at the SOLEIL (beamline CRISTAL) proposal No. 20210474.

Supplementary material. The supplementary material for this article can be found at https://doi.org/10.1180/mgm.2024.22.

Competing interests. The authors declare none.

References

Angyan J., Jansen G., Loos M., Hattig C. and Hess B. (1994) Distributed polarizabilities using the topological theory of atoms in molecules. *Chemical Physics Letters*, **219**, 267–273.

Bader R.F.W. (1994) *Atoms in Molecules: A Quantum Theory*. International Series of Monographs on Chemistry, Oxford University Press, Oxford, UK, 456 pp.

Bader R.F.W. (2006) Comment on the comparative use of the electron density and its Laplacian. *Chemistry – A European Journal*, **12**, 7769–7772.

Becke A. (1993) Density-Functional Thermochemistry 3. The role of exact exchange. *Journal of Chemical Physics*, **98**, 5648–5652.

Blessing R. (1995) An empirical correction for absorption anisotropy. *Acta Crystallographica*, **A51**, 33–38.

Bolotina N.B., Molchanov V.N., Dyuzheva T.I., Lityagina L.M. and Bendeliani N.A. (2008) Single-crystal structures of high-pressure phases FeOOH, FeOOD, and GaOOH. *Crystallography Reports*, **53**, 960–965.

Busing W. and Levy H. (1958) A single crystal neutron diffraction study of diaspore, AlO(OH). *Acta Crystallographica*, **11**, 798–803.

Cedillo A., Torrent M. and Cortona P. (2016) Stability of the different AlOOH phases under pressure. *Journal of Physics-Condensed Matter*, **28**, 185401.

Coppens P. and Coppens P. (1997) *X-Ray Charge Densities and Chemical Bonding*. International Union of Crystallography Texts on Crystallography, Oxford University Press, Oxford, UK, 372 pp.

Coppens P., Gururow T., Leung P., Stevens E., Becker P. and Yang Y. (1979) Electron population analysis of accurate diffraction data. 7. Net atomic charges and molecular dipole-moments from spherical-atom X-ray refinements, and the relation between atomic charge and shape. *Acta Crystallographica*, **A35**, 63–72.

Cortona P. (2017) Hydrogen bond symmetrization and elastic constants under pressure of delta-AlOOH. *Journal of Physics-Condensed Matter*, **29**, 325505.

CrysAlis Pro (2014) *CrysAlisPro Software system*. Agilent Technologies Ltd, Yarnton, Oxfordshire, England.

Dolomanov O.V., Bourhis L.J., Gildea R.J., Howard J.A.K. and Puschmann H. (2009) OLEX2: a complete structure solution, refinement and analysis program. *Journal of Applied Crystallography*, **42**, 339–341.

Dovesi R., Orlando R., Civalleri B., Roetti C., Saunders V.R. and Zicovich-Wilson C.M. (2005) CRYSTAL: a computational tool for the ab initio study of the electronic properties of crystals. *Zeitschrift Fur Kristallographie*, **220**, 571–573.

Dovesi R., Erba A., Orlando R., Zicovich-Wilson C.M., Civalleri B., Maschio L., Rérat M., Casassa S., Baima J., Salustro S. and Kirtman B. (2018) Quantum-mechanical condensed matter simulations with CRYSTAL. *Computational Molecular Science*, **8**, e1360.

Erba A., Ferrabone M., Orlando R. and Dovesi R. (2013) Accurate dynamical structure factors from ab initio lattice dynamics: The case of crystalline silicon. *Journal of Computational Chemistry*, **34**, 346–354.

Ewing F.J. (1935) The crystal structure of diaspore. *The Journal of Chemical Physics*, **3**, 203–207.

Farrugia L.J. (2012) WinGX and ORTEP for Windows: an update. *Journal of Applied Crystallography*, **45**, 849–854.

Friedrich A., Wilson D.J., Haussuehl E., Winkler B., Morgenroth W., Refson K. and Milman V. (2007a) High-pressure properties of diaspore, AlO(OH). *Physics and Chemistry of Minerals*, **34**, 145–157.

Friedrich A., Haussuehl E., Boehler R., Morgenroth W., Juarez-Arellano E.A. and Winkler B. (2007b) Single-crystal structure refinement of diaspore at 50 GPa. *American Mineralogist*, **92**, 1640–1644.

Gajda R., Stachowicz M., Makal A., Sutula S., Parafiniuk J., Fertey P. and Wozniak K. (2020) Experimental charge density of grossular under pressure – a feasibility study. *IUCRJ*, **7**, 383–392.

Gajda R., Zhang D., Parafiniuk J., Dera P. and Wozniak K. (2022) Tracing electron density changes in langbeinite under pressure. *IUCRJ*, **9**, 146–162.

Grevel K.D., Burchard M., Fasshauer D.W. and Peun T. (2000) Pressure-volume-temperature behavior of diaspore and corundum: An in situ X-ray diffraction study comparing different pressure media. *Journal of Geophysical Research-Solid Earth*, **105**, 27877–27887.

Grimme S., Antony J., Ehrlich S. and Krieg H. (2010) A consistent and accurate ab initio parametrization of density functional dispersion correction (DFT-D) for the 94 elements H-Pu. *The Journal of Chemical Physics*, **132**, 154104.

Hahn Th. (editor) (2002) *International Tables for Crystallography, Volume A: Space Group Symmetry*. Published for the International Union of Crystallography by Kluwer Academic Publishers, London.

Hansen N. and Coppens P. (1978) Electron population analysis of accurate diffraction data 6. Testing aspherical atom refinements on small-molecule data sets. *Acta Crystallographica*, **A34**, 909–921.

Hill R. (1979) Crystal-structure refinement and electron-density distribution in diaspore. *Physics and Chemistry of Minerals*, **5**, 179–200.

Huang S., Xu J., Liu D., Li B., Ye Z., Chen W., Kuang Y., Chi F., Fan D., Ma M. and Zhou W. (2021) Stability and thermoelasticity of diaspore by synchrotron x-ray diffraction and Raman spectroscopy. *Frontiers in Earth Science*, **9**, 752566.

Ito Y., Ikeda O., Ban R., Kubota T., Sakamaki T., Kuribayashi T. and Suzuki A. (2021) Phase transitions of ScOOH under high pressure. *High Pressure Research*, **41**, 275–289.

Ito Y., Ikeda O., Sakamaki T., Kuribayashi T. and Suzuki A. (2022) P-V-T equation of state of alpha-ScOOH. *High Pressure Research*, **42**, 200–212.

Kang D., Feng Y.-X., Yuan Y., Ye Q.-J., Zhu F., Huo H.-Y., Li X.-Z. and Wu X. (2017) Hydrogen-bond symmetrization of delta-AlOOH. *Chinese Physics Letters*, **34**, 108301.

Ketkaew R., Tantirungrotechai Y., Harding P., Chastanet G., Guionneau P., Marchivie M. and Harding D.J. (2021) OctaDist: a tool for calculating distortion parameters in spin crossover and coordination complexes. *Dalton Transactions*, **50**, 1086–1096.

Komatsu K., Kuribayashi T., Sano A., Ohtani E. and Kudoh Y. (2006) Redetermination of the high-pressure modification of AlOOH from single-crystal synchrotron data. *Acta Crystallographica*, **E62**, I216–I218.

Kuribayashi T., Sano-Furukawa A. and Nagase T. (2014) Observation of pressure-induced phase transition of delta-AlOOH by using single-crystal synchrotron X-ray diffraction method. *Physics and Chemistry of Minerals*, **41**, 303–312.

Lee C., Yang W. and Parr R.G. (1988) Development of the Colle-Salvetti correlation-energy formula into a functional of the electron density. *Physical Review. B, Condensed Matter*, **37**, 785–789.

Li M., Snoussi K., Li L., Wang H., Yang W. and Gao C. (2010) Diaspore crystal structure and compressibility at high pressures and high temperature. *Applied Physics Letters*, **96**, 261902.

Li X., Speziale S., Koch-Mueller M., Husband R.J. and Liermann H.-P. (2022) Phase stability of Al-bearing dense hydrous magnesium silicates at topmost lower mantle conditions: Implication for water transport in the mantle. *Geophysical Research Letters*, **49**, e2022GL098353.

Lufaso M.W. and Woodward P.M. (2004) Jahn–Teller distortions, cation ordering and octahedral tilting in perovskites. *Acta Crystallographica*, **B60**, 10–20.

Luo C., Umemoto K. and Wentzcovitch R.M. (2022) Ab initio investigation of H-bond disordering in delta-AlOOH. *Physical Review Research*, **4**, 023223.

Momma K and Izumi F (2011) VESTA 3 for three-dimensional visualization of crystal, volumetric and morphology data. *Journal of Applied Crystallography*, **44**, 1272–1276.

Ohira I., Ohtani E., Sakai T., Miyahara M., Hirao N., Ohishi Y. and Nishijima M. (2014) Stability of a hydrous δ-phase, AlOOH-$MgSiO_2(OH)_2$, and a mechanism for water transport into the base of lower mantle. *Earth And Planetary Science Letters*, **401**, 12–17.

Pawley A.R., Redfern S. a. T. and Holland T.J.B. (1996) Volume behavior of hydrous minerals at high pressure and temperature .1. Thermal expansion of lawsonite, zoisite, clinozoisite, and diaspore. *American Mineralogist*, **81**, 335–340.

Pillai S.B., Jha P.K., Padmalal A., Maurya D.M. and Chamyal L.S. (2018) First principles study of hydrogen bond symmetrization in delta-AlOOH. *Journal of Applied Physics*, **123**, 115901.

Popelier P.L.A. (1996) Integration of atoms in molecules: A critical examination. *Molecular Physics*, **87**, 1169–1187.

Sanjuan-Szklarz W.F., Woinska M., Domagala S., Dominiak P.M., Grabowsky S., Jayatilaka D., Gutmann M. and Wozniak K. (2020) On the accuracy and precision of X-ray and neutron diffraction results as a function of resolution and the electron density model. *IUCRJ*, **7**, 920–933.

Sano-Furukawa A., Komatsu K., Vanpeteghem C.B. and Ohtani E. (2008) Neutron diffraction study of delta-AlOOD at high pressure and its implication for symmetrization of the hydrogen bond. *American Mineralogist*, **93**, 1558–1567.

Sano-Furukawa A., Kagi H., Nagai T., Nakano S., Fukura S., Ushijima D., Iizuka R., Ohtani E. and Yagi T. (2009) Change in compressibility of delta-AlOOH and delta-AlOOD at high pressure: A study of isotope effect and hydrogen-bond symmetrization. *American Mineralogist*, **94**, 1255–1261.

Sano-Furukawa A., Yagi T., Okada T., Gotou H. and Kikegawa T. (2012) Compression behaviors of distorted rutile-type hydrous phases, MOOH (M = Ga, In, Cr) and CrOOD. *Physics and Chemistry of Minerals*, **39**, 375–383.

Sano-Furukawa A., Hattori T., Komatsu K., Kagi H., Nagai T., Molaison J.J., dos Santos A.M. and Tulk C.A. (2018) Direct observation of symmetrization of hydrogen bond in delta-AlOOH under mantle conditions using neutron diffraction. *Scientific Reports*, **8**, 15520.

Sheldrick G.M. (2008) A short history of SHELX. *Acta Crystallographica*, **A64**, 112–122.

Sheldrick G.M. (2015) Crystal structure refinement with SHELXL. *Acta Crystallographica*, **C71**, 3–8.

Shito C., Okamoto K., Sato Y., Watanabe R., Ohashi T., Fuchizaki K., Kuribayashi T. and Suzuki A. (2019) In-situ X-ray diffraction study on beta-CrOOH at high pressure and high-temperature. *High Pressure Research*, **39**, 499–508.

Simonova D., Bykova E., Bykov M., Kawazoe T., Simonov A., Dubrovinskaia N. and Dubrovinsky L. (2020) Structural study of delta-AlOOH up to 29 GPa. *Minerals*, **10**, 1055.

Stachowicz M., Gajda R., Huć A., Parafiniuk J., Makal A., Sutuła S., Fertey P. and Woźniak K. (2023) Charge density redistribution with pressure in a zeolite framework. *Scientific Reports*, **13**, 1609.

Su Z. and Coppens P. (1997) Relativistic X-ray elastic scattering factors for neutral atoms Z=1-54 from multi-configuration Dirac-Fock wavefunctions in the 0-12 $Å^{-1}$ sin θ/λ range, and six-Gaussian analytical expressions in the 0-6 Å–1 range. *Acta Crystallographica*, **A53**, 749–762.

Sugiura T., Arima H., Nagai T. and Sugiyama K. (2018) Structural variations accompanied by thermal expansion of diaspore: in-situ single-crystal and powder X-ray diffraction study. *Physics and Chemistry of Minerals*, **45**, 1003–1010.

Suzuki A. (2013) Compression behavior of manganite. *Journal of Mineralogical and Petrological Sciences*, **108**, 295–299.

Suzuki A. (2018) P-V-T equation of state of rhodium oxyhydroxide. *High Pressure Research*, **38**, 145–152.

https://doi.org/10.1180/mgm.2024.22 Published online by Cambridge University Press

Suzuki A. (2022) In situ X-ray diffraction study of the phase boundary between diaspore and ?-AlOOH. *Journal of Mineralogical and Petrological Sciences*, **117**, 002.

Suzuki A., Ohtani E. and Kamada T. (2000) A new hydrous phase delta-AlOOH synthesized at 21 GPa and 1000 degrees C. *Physics and Chemistry of Minerals*, **27**, 689–693.

Tang S., Huang X., Zhang J. and Cui Q. (2020) InOOH bulk crystals and ultrathin nanowires under compression. *Acs Omega*, **5**, 15146–15151.

Thompson E.C., Campbell A.J. and Tsuchiya J. (2021) Elastic properties of the pyrite-type FeOOH-AlOOH system from first-principles calculations. *Geochemistry Geophysics Geosystems*, **22**, e2021GC009703.

Trybel F., Meier T., Wang B. and Steinle-Neumann G. (2021) Absence of proton tunneling during the hydrogen-bond symmetrization in delta-AlOOH. *Physical Review B*, **104**, 104311.

Tsuchiya J., Tsuchiya T., Tsuneyuki S. and Yamanaka T. (2002) First principles calculation of a high-pressure hydrous phase, delta-AlOOH. *Geophysical Research Letters*, **29**, 1909.

Verma A.K., Modak P. and Stixrude L. (2018) New high-pressure phases in MOOH (M = Al, Ga, In). *American Mineralogist*, **103**, 1906–1917.

Vilela Oliveira D., Laun J., Peintinger M.F. and Bredow T. (2019) BSSE-correction scheme for consistent gaussian basis sets of double- and triple-zeta valence with polarization quality for solid-state calculations. *Journal of Computational Chemistry*, **40**, 2364–2376.

Volkov A., Macchi P., Farrugia L., Gatti C., Mallinson P., Richter T. and Koritsanszky T. (2016) *XD2016 – A Computer Program Package for Multipole Refinement, Topological Analysis of Charge Densities and Evaluation of Intermolecular Energies from Experimental and Theoretical Structure Factors*.

Xu J., Hu J., Ming L., Huang E. and Xie H. (1994) The compression of diaspore, AlO(OH) at room-temperature up to 27 Gpa. *Geophysical Research Letters*, **21**, 161–164.

Xu C., Inoue T., Kakizawa S., Noda M. and Gao J. (2021) Effect of Al on the stability of dense hydrous magnesium silicate phases to the uppermost lower mantle: implications for water transportation into the deep mantle. *Physics and Chemistry Of Minerals*, **48**, 31.

Zhang L., Ying F., Wu W., Hiberty P.C. and Shaik S. (2009) Topology of electron charge density for chemical bonds from valence bond theory: a probe of bonding types. *Chemistry – A European Journal*, **15**, 2979–2989.

Zhang Z., Cui H., Yang D.-P., Zhang J., Tang S.-X., Wu S. and Cui Q.-L. (2017) Anomalous behavior and phase transformation of alpha-GaOOH nanocrystals under static compression. *Chinese Physics B*, **26**, 106402.

https://doi.org/10.1180/mgm.2024.22 Published online by Cambridge University Press